International Journal of Nanomedicine

Dovepress
open access to scientific and medical research

Open Access Full Text Article

ORIGINAL RESEARCH

Optimizing the Biocompatibility of PLLA Stent Materials: Strategy with Biomimetic Coating

Hao Du[1], Wentao Li[1], Xueyi Li[2], Zhiyuan Qiu[1], Jie Ding[2], Yi Zhang[1]

[1]Center of Interventional Radiology and Vascular Surgery, Department of Radiology, Cultivation and Construction Site of the State Key Laboratory of Intelligent Imaging and Interventional Medicine, Basic Medicine Research and Innovation Center of Ministry of Education, Zhongda Hospital, Medical School, Southeast University, Nanjing, Jiangsu Province, People's Republic of China; [2]Department of Biochemistry and Molecular Biology, Medical School, Southeast University, Nanjing, Jiangsu Province, People's Republic of China

Correspondence: Jie Ding; Yi Zhang, Email dingjie711@seu.edu.cn; yizhangcir@126.com

Background: Poly-L-lactic acid (PLLA) stents have broad application prospects in the treatment of cardiovascular diseases due to their excellent mechanical properties and biodegradability. However, foreign body reactions caused by stent implantation remain a bottleneck that limits the clinical application of PLLA stents. To solve this problem, the biocompatibility of PLLA stents must be urgently improved. Albumin, the most abundant inert protein in the blood, possesses the ability to modify the surface of biomaterials, mitigating foreign body reactions—a phenomenon described as the "stealth effect". In recent years, a strategy based on albumin camouflage has become a focal point in nanomedicine delivery and tissue engineering research. Therefore, albumin surface modification is anticipated to enhance the surface biological characteristics required for vascular stents. However, the therapeutic applicability of this modification has not been fully explored.

Methods: Herein, a bionic albumin (PDA-BSA) coating was constructed on the surface of PLLA by a mussel-inspired surface modification technique using polydopamine (PDA) to enhance the immobilization of bovine serum albumin (BSA).

Results: Surface characterization revealed that the PDA-BSA coating was successfully constructed on the surface of PLLA materials, significantly improving their hydrophilicity. Furthermore, in vivo and in vitro studies demonstrated that this PDA-BSA coating enhanced the anticoagulant properties and pro-endothelialization effects of the PLLA material surface while inhibiting the inflammatory response and neointimal hyperplasia at the implantation site.

Conclusion: These findings suggest that the PDA-BSA coating provides a multifunctional biointerface for PLLA stent materials, markedly improving their biocompatibility. Further research into the diverse applications of this coating in vascular implants is warranted.

Keywords: vascular stent, Poly-L-lactic acid, albumin, biomimetic coating, stealth effect

Introduction

Cardiovascular diseases (CVDs) are increasingly becoming the leading cause of death worldwide, resulting in a serious public health burden.[1] Interventional therapy, which involves endovascular stenting (ES), is the most widespread and effective method for treating CVDs.[2,3] Currently, commonly used bare metal stents (BMSs) and drug-eluting stents (DESs) are made with nonbiodegradable metal materials and can support the initial stage of implantation to maintain vascular patency.[4,5] However, the risk of thrombosis and restenosis are often increased by permanent stent retention, which also hinders imaging evaluations and further clinical intervention.[6,7] Bioabsorbable vascular stents (BVSs) are becoming a new strategy to improve the long-term outcome of ES as BVSs degrade over time after they perform their supportive role, which facilitates revascularization and functional recovery.[8] Poly-L-lactic Acid (PLLA) is an ideal material for BVS due to its excellent biodegradability and mechanical properties;[9] in addition, PLLA has shown good degradation behavior and biosafety in clinical trials, with additional clinical evidence supporting its application.[10,11] Nevertheless, PLLA stents inevitably cause a foreign body reaction in host tissues, affecting the therapeutic efficacy of ES.[10,12] This reaction is attributed to platelet adhesion and immune cell activation, which occurs when the stent is sensed as an intravascular;[13,14] as

Received: 2 February 2024
Accepted: 23 May 2024
Published: 4 June 2024

Graphical Abstract

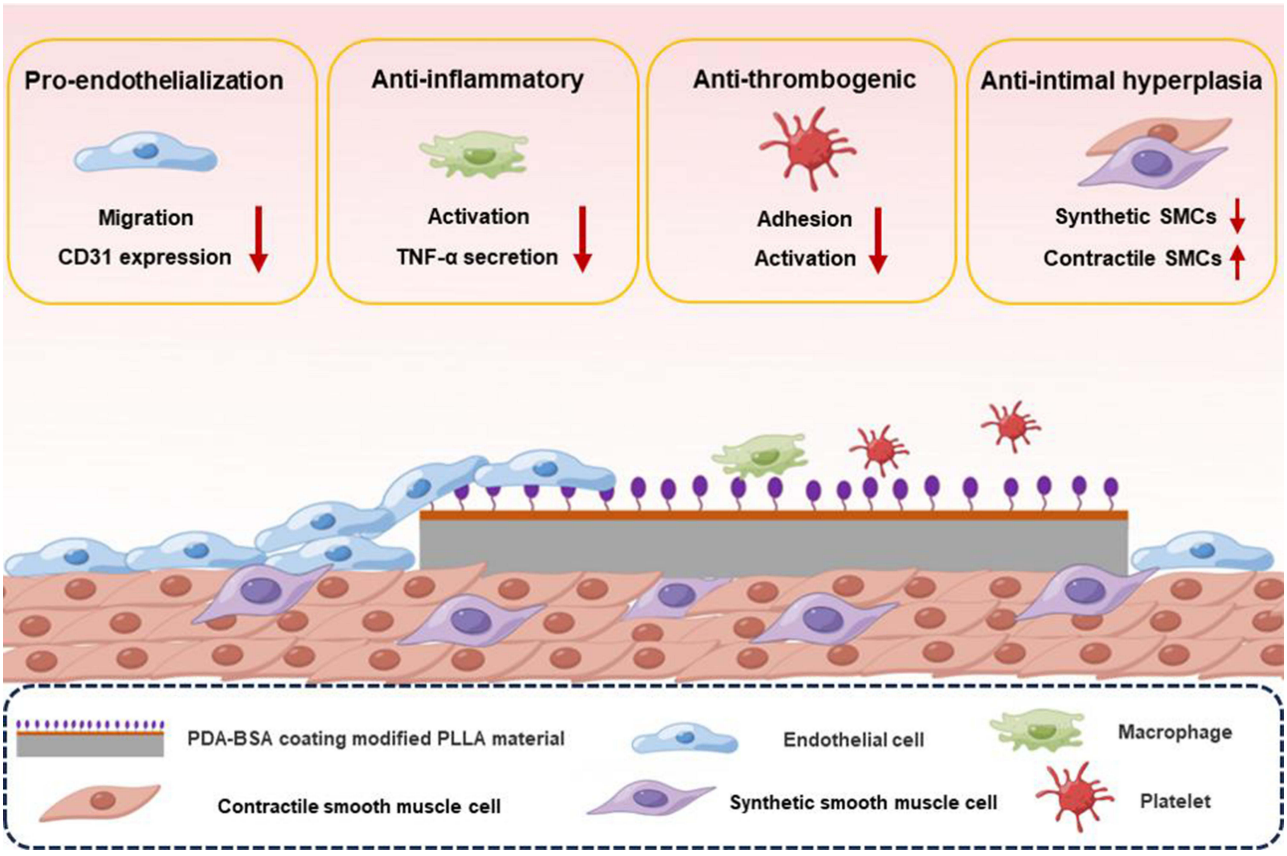

a result, in-stent thrombosis and intimal hyperplasia ultimately occur. For these reasons, the interface between the PLLA stent and host tissue must be improved to mitigate foreign body reactions and achieve long-term patency and definitive efficacy of ES. In this context, a simple and effective camouflage strategy that involves "stealth" modifications of vascular implanted foreign bodies (eg, coating with natural biomaterials) deserves further investigation.

Albumin is the most abundant plasma protein in the blood and is usually a nonadhesive protein.[15] In recent years, albumin has been widely used in clinical and biomedical research due to its superior intrinsic properties, such as biocompatibility, biodegradability and low immunogenicity.[16] Notably, albumin can blunt the surface of biomaterials and is an effective immune escape coating because surface albumin prevents other adhesive proteins (especially fibrinogen) from nonspecifically adsorbing on the surface of a material, inhibiting blood coagulation and inflammatory responses.[17–19] To date, the albumin camouflage strategy has attracted much attention in the field of nanomedicine delivery and tissue engineering.[20] Albumin-coated nanoparticles (eg, liposomes,[21] DNA origami,[22] and metal nanoparticles[23]) resist phagocytosis by the immune system and prevent other plasma proteins from adsorbing on the nanoparticle surfaces, thereby prolonging their circulation time in the blood. Furthermore, in the field of tissue engineering, Kenry et al[24] reported that albumin-functionalized graphene oxide (GO) couplings showed enhanced antithrombotic effects and may serve as a coating material for blood-contacting devices. Tao et al[25] reported that the transplantation of albumin-coated porcine hyaline cartilage scaffolds into rat omentum attenuated immune and inflammatory responses to xenografts. Although the albumin-coated stealth effect shows great potential to improve the performance of vascular implants (vascular grafts and stents), its therapeutic applicability in vascular implants has not been fully explored at this time. Given this background, we sought to apply albumin camouflage strategies to enhance the biocompatibility of PLLA vascular stents.

However, the inert PLLA material lacks reactive groups on its surface and cannot directly immobilize albumin.[26] Therefore, preliminary surface modification of PLLA materials is necessary to provide additional reactive active groups for albumin immobilization. Polydopamine (PDA), a bonding polymer inspired by marine mussels, can be used to modify the surface of a variety of materials due to its strong adhesion properties and biocompatibility characteristics.[27,28] Previous studies have shown that PDA coatings improve endothelial cell function and inhibit vascular smooth muscle cell adhesion and proliferation, making them promising candidates for "pro-healing" coatings for vascular implants.[29,30] More importantly, PDA coatings with reactive groups can be used as secondary reaction platforms to further graft biofunctional molecules.[31,32] Thus, the immobilization of albumin onto the PDA coating platform is expected to synergistically contribute to the surface biological properties necessary for PLLA vascular stents, such as thromboprotection, anti-inflammatory effects, and pro-endothelialization.

In this study, we constructed a biomimetic albumin (PDA-BSA) coating with a multifunctional biointerface by stably immobilizing bovine serum albumin (BSA) on the surface of a PDA-coated modified PLLA stent material via covalent bond coupling. To demonstrate this phenomenon, we first systematically characterized the physicochemical properties of the coating. Then, we conducted a series of in vivo and in vitro experiments to evaluate the endothelialization, anti-thrombogenic, inhibits intimal proliferation, and regulates inflammation effects of the coating, thus analyzing its impact on the biocompatibility of PLLA.

Materials and Methods

Materials

Poly-L-lactic acid (PLLA, Mw = 537 kDa) was purchased from Evonik Industries AG (Essen, Germany). Dopamine, Tris (hydroxymethyl) aminomethane (Tris-base) and bovine serum albumin (BSA, purity ≥ 98%) were purchased from Sigma–Aldrich (USA). Human umbilical vein endothelial cells (HUVECs) and RAW264.7 macrophages were purchased from Pricella (China). Sprague–Dawley (SD) rats and New Zealand white rabbits were obtained from Shanghai BK/KY Biotechnology Co., Ltd (China). All animal experiments were approved by the Institutional Animal Care and Use Committee of the Medical School of Southeast University (approval ID: SYXK-2021.0022), according to Laboratory Animal—Guideline for Ethical Review of Animal Welfare (GB/T 35,892-2018).

Preparation of PLLA Membranes and Monofilaments

PLLA Film Preparation

A 2.5% (w/v) PLLA solution was prepared by dissolving PLLA powder in chloroform with constant magnetic stirring for 6 h at room temperature. The solution was then cast in glass dishes and evaporated in a set vacuum oven at 25°C for 48 h to obtain PLLA films of uniform thickness. Finally, the resulting PLLA membrane was washed several times with ethanol and deionized water to remove any residual solvent, and then the membrane sample was dried under a stream of nitrogen.

PLLA Monofilament Preparation

PLLA powder was melted and extruded through a single-screw extruder (HIGHRICHJA EXTRUSION, HRJSJ-Φ20) to produce 0.6 ± 0.02 mm virgin PLLA monofilaments. The extruded monofilaments were solid-state drawn at 85–120°C to form monofilaments with a diameter of approximately 150 mm. The details of the process can be found in a previously published article.[33]

Preparation of the PLLA Surface Coatings

A dopamine solution with a concentration of 2.0 mg/mL was prepared by adding dopamine to Tris-HCl buffer solution (10 mM, pH 8.5). The PLLA substrates were immersed in dopamine solution and shaken at 37°C for 24 hours. Then, the mixture was removed and washed thoroughly with deionized water to remove the dark brown precipitate on the surface. The mixture was dried in a vacuum oven at 37°C for 12 h to generate a PLLA substrate with a PDA coating labeled PLLA/PDA. Next, the PLLA/PDA substrate was immersed in a 2 mg/mL BSA solution (in PBS) with a pH of 7.8 and reacted at 4°C for 24 h. Subsequently, the substrate was washed thoroughly with ionized water, washed thoroughly and dried at 37°C for 12 h to prepare the final sample labeled PLLA/PDA-BSA. The preparation process of the coating is shown schematically in Figure 1.

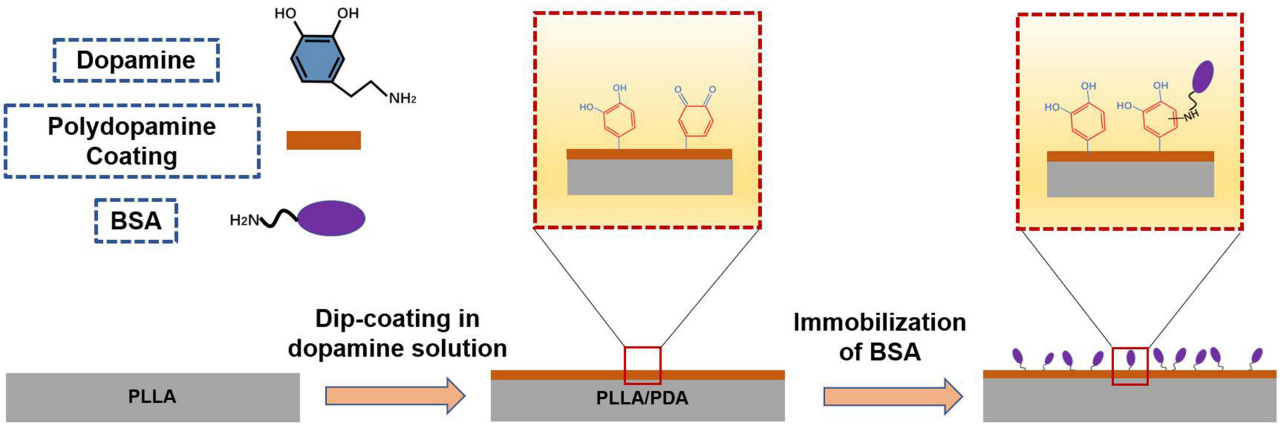

Figure 1 Preparation of a PDA-BSA coating on the surface of PLLA material. A thin polydopamine layer was coated on the PLLA substrate by immersing the PLLA substrate in an aqueous dopamine solution for a period. And then BSA was covalently grafted onto the resultant PLLA/PDA composite membranes by the coupling between o-benzoquinone and BSA amine.

Coatings Characterization

Attenuated total reflection Fourier transform infrared spectroscopy (ATR-FTIR, Bruker-Vetor 22, Germany), operated in a wavenumber range of 500–4000 cm-1, was applied to characterize the surface chemical bonds. The surface element compositions of the coatings were analyzed through X-ray photoelectron spectroscopy (XPS; Thermo Scientific-Escalab 250Xi, USA). The roughness of the surface was detected using atomic force microscopy (AFM; Bruker-Dimension ICON, Germany) in tapping mode with a scanned range of 20 μm × 20 μm. The surface morphology was evaluated using a scanning electron microscope (SEM; Zeiss-sigma 300, Germany), and the distribution of elements on the PLLA/PDA-BSA surface was determined via energy dispersive X-ray spectroscopy (EDS). The coated surfaces were observed by a contact angle goniometer (LAUDA Scientific, Germany) to assess their hydrophilicity.

Endothelial Cell Culture and Analysis

Human umbilical vein endothelial cells (HUVECs; Pricella, Wuhan, China) were used to investigate the effects of different membrane samples on endothelial cell growth and function. Briefly, membrane samples (1 cm × 1 cm) were placed in 24-well culture plates, and HUVECs were inoculated at a density of 5 × 10^4 cells/mL. The cells were incubated in a 37°C cell culture incubator (95% air, 5% CO2) for 4 hours and 3 days. Cell adhesion and proliferation were detected at hour 4 and day 3 using a Cell Counting Kit-8 (CCK-8) assay. The samples were then fixed and stained with an anti-platelet endothelial cell adhesion molecule-1 antibody (CD31; Abcam, UK) and DAPI (Sigma, USA) and observed under an inverted fluorescence microscope (Olympus, Japan). The fluorescence signal intensity of the CD31 image was analyzed using ImageJ software.

Inflammatory Response Analysis

Macrophage Adherence Analysis

To assess the inflammatory response in vitro, RAW264.7 (Pricella, Wuhan, China) macrophages were inoculated onto membrane samples (1 cm × 1 cm) at a density of 5 × 10^4 cells/mL and cultured under standard culture conditions for 3 days, after which the morphology of the macrophages on the surface of the samples was observed via light microscopy. Macrophage culture supernatants were collected, and the secretion of the proinflammatory factor TNF-α was detected via enzyme-linked immunosorbent assay (ELISA).

In vivo Subcutaneous Implantation

To assess local inflammation in the tissues surrounding the in vivo sample implants, subcutaneous implantation of the samples was performed on the backs of rats to explore the inflammatory response.[34] Three male Sprague–Dawley (SD) rats (280–300 g) were anesthetized by intraperitoneal injection of sodium pentobarbital (40 mg-kg-1). Three incisions were created in the back of each rat, and three sets of different membrane samples (1 cm × 1 cm) were placed in separate subcutaneous pockets. After 4 weeks,

samples with surrounding tissue were collected to assess the tissue inflammatory response. The tissues were fixed with paraformaldehyde, embedded in paraffin and stained with hematoxylin and eosin (H&E) for further study.

Blood Compatibility Analysis

Hemolysis Rate

A hemolysis test was performed using a rabbit erythrocyte suspension according to the reported protocol.[35] Rabbit whole blood was mixed with 0.9% (w/v) sodium chloride solution at a 4:5 ratio. Prior to testing, all samples were immersed in centrifuge tubes containing 10 mL of saline and incubated for 30 min at 37°C. Ten milliliters of 0.9 (w/v) saline or deionized water was used as a negative or positive control, respectively. Then, 0.2 mL of blood was added to each centrifuge tube, and the samples were incubated at 37°C for 1 hour. Subsequently, the samples were removed, and all centrifuge tubes were centrifuged at 3000 rpm for 5 min. Then, 150 μL of supernatant from the centrifuge tubes was carefully pipetted into a 96-well plate, and the absorbance was read and recorded at 540 nm by an enzyme meter. The hemolysis rate was calculated as follows:

$$\text{Hemolysis Ratio}\,(\%) = [(\text{A} - \text{C1})/(\text{C2} - \text{C1})] \times 100\%$$

where A is the absorbance of the sample, C_1 is the absorbance of the negative control and C_2 is the absorbance of the positive control.

In vitro Evaluation of Platelet Adhesion and Activation

Platelet-rich plasma (PRP) was prepared by centrifuging 3.8 wt% sodium citrate-anticoagulated rabbit whole blood at 1500 rpm for 15 min. Then, 100 μL of PRP was added to the surface of the membrane samples (1 cm × 1 cm), and the samples were incubated at 37°C for 1 h. Afterward, the unadhered platelets were removed by moderate shaking in PBS. Platelets that adhered to the sample surface were fixed in 2.5% glutaraldehyde solution overnight, dehydrated through an ethanol gradient, and visualized via SEM. In addition, adherent platelets were quantified using a lactate dehydrogenase (LDH) release assay kit (Beyotime, Shanghai, China).

Ex vivo Circulation Thrombogenicity Test

The following experiments were performed according to previously reported guidelines.[36] Under general anesthesia, three adult New Zealand Large White rabbits (3–3.5 kg) were isolated by dividing the left carotid artery and the right jugular vein and puncturing them with an indwelling needle. The membrane samples (0.8 cm × 1 cm) were coiled and placed in parallel into heparinized medical polyvinyl chloride (PVC) catheters, which were assembled with an indwelling needle. An extracorporeal circulatory pathway was established by connecting the vessel to the catheter. Two hours later, the blood flow rate was monitored, the circulatory pathway was disconnected, and a cross-section of the catheter was photographed. The thrombus attached to the surface of the sample was collected, photographed, and weighed. The samples were then rinsed with saline (0.9%). and fixed with glutaraldehyde solution (2.5%) overnight. The surface thrombi of all samples were dehydrated by gradient ethanol and observed via SEM.

In vivo Vascular Biocompatibility Assessment: Monofilament Sample Implantation

Uncoated, PDA, and PDA/BSA-coated PLLA monofilaments (Φ0.15 mm×10 mm) were implanted into the lumen of the carotid arteries of SD rats (n=3) to mimic the presence of a stent strut.[37] After 28 days, the carotid arteries of the rats were imaged via MSME-PD-T2 sequences on a 7T small animal magnetic resonance imaging (MRI, Bruker, Germany). Subsequently, the rats were euthanized, and the carotid arteries that contained the implanted monofilaments were harvested and stained with H&E, anti-CD31, anti-α-SMA, and anti-OPN antibodies for histological analysis.

Statistical Analysis

All experiments were performed at least three times, and the results are expressed as the mean ± standard deviation (SD). One-way analysis of variance (ANOVA) was used to analyze the experimental results, and a p value < 0.05 was considered to indicate a significant difference between two groups.

Results and Discussion

Surface Characterization

We used ATR-FTIR to analyze the chemical structure of the samples. As shown in Figure 2A, the characteristic peaks at approximately 1750 cm-1 and 2950 cm-1 were attributed to the carbonyl group stretching and the O-H asymmetric vibration of PLLA, respectively. After modification with the PDA coating, the characteristic peaks of PLLA significantly contracted, and some new absorption peaks appeared at approximately 1615 cm-1 (superposition of N-H bending and phenyl C=C stretching) and 1510 cm-1 (N-H shear), which demonstrated that there was a PDA layer on the PLLA membrane. The new absorption peak at ~3000-3600 cm-1 after modification with BSA was attributed to the N-H stretching vibration of BSA and indicated that the PLLA/PDA surface was successfully modified with BSA. To further confirm the modification, XPS further verified the changes in the elemental content of the sample surface, as shown in Figure 2B; only the C 1s and O 1s elemental peaks were present in the PLLA group. However, N1s peaks appeared after the PDA coating process, indicating that the PDA coating was successfully modified on the PLLA surface. In addition, the N1s peak increased after further modification with BSA, and a new sulfur (S2p) peak appeared, which indicated that BSA was successfully grafted onto the PLLA/PDA surface.

The surface morphology and roughness of the samples were observed via AFM and SEM after modification. Figure 2C shows the 2D and 3D micromorphology images characterized by AFM. The coating modification resulted in significant changes in the topography and roughness of the PLLA. The smooth surface of PLLA became rough due to polydopamine deposition. Further grafting of BSA reduced the surface roughness of the PDA coating. The average roughnesses (Ra) of PLLA, PLLA/PDA and PLLA/PDA-BSA samples were 39.0 nm, 195 nm, and 41.4 nm, respectively. SEM further revealed the differences in the surface morphology of the samples as shown in Figure 2D. Compared with the PLLA samples, a dense coating with tiny cracks can be observed on the surface of the PLLA/PDA samples, which is mainly due to the self-polymerization of dopamine. The introduction of BSA did not cause a significant change in the surface morphology of PLLA/PDA samples, but the cracks in the PLLA/PDA-BSA surface coatings were relatively reduced, which resulted in a more homogeneous and dense coating. The EDS elemental mappings (Figure 2E) illustrated the distribution and density of carbon, oxygen, nitrogen, and sulfur on the surface of the PDA-BSA coatings, distribution and density. Theoretically, sulfur is a characteristic element of BSA in our system, which was confirmed by our XPS results (Figure 2B). The EDS elemental distributions showed that sulfur was uniformly distributed on the PLLA/PDA-BSA surface, which suggested that BSA was successfully immobilized on the PLLA/PDA surface.

The hydrophilic properties of the samples were characterized by measuring the water contact angle. As shown in Figure 2F, the WCA of the PLLA membrane was 102.7 ± 1.2°, and the WCA was reduced to 53.7 ± 1.6° after PDA modification, which was attributed to the presence of many imine and phenolic hydroxyl groups in the PDA molecule. When BSA was further immobilized on the PLLA/PDA membrane, the WCA decreased to 43.0 ± 1.7°, suggesting that the grafting of BSA may increase the hydrophilicity of the PDA coating. PLLA is a hydrophobic material, and undergoing PDA and PDA/BSA coating modifications ultimately resulted in an increase in the hydrophilicity of PLLA. Due to this change, protein adsorption may be reduced, and biocompatibility may be improved, as discussed in the following sections.

Investigation of Endothelial Cell Proliferation and Functionality

Endothelial cells (ECs) are the major cellular component of vascular tissue, and it is physiologically important to assess their growth behavior on the surface of stent materials.[38] For example, incomplete EC healing or impaired function after vascular stent implantation increases the risk of thrombosis and restenosis.[39] In this work, the proliferation and functionalization of ECs on different coatings after 4 h and 3 days were investigated by immunofluorescence staining (for CD31 (green) and DAPI (blue)) and cell viability tests, respectively. Compared with the PLLA group, the PLLA/PDA and PLLA/PDA-BSA groups significantly promoted the adhesion and proliferation of ECs (Figure 3A and B). CD31 is a specific marker for vascular ECs and plays an important role in maintaining the normal function of ECs and homeostasis of the vascular microenvironment. Upregulation or downregulation of CD31 expression indicates an increase or a decrease in EC function, respectively.[37] In the present study, we analyzed CD31 expression by measuring

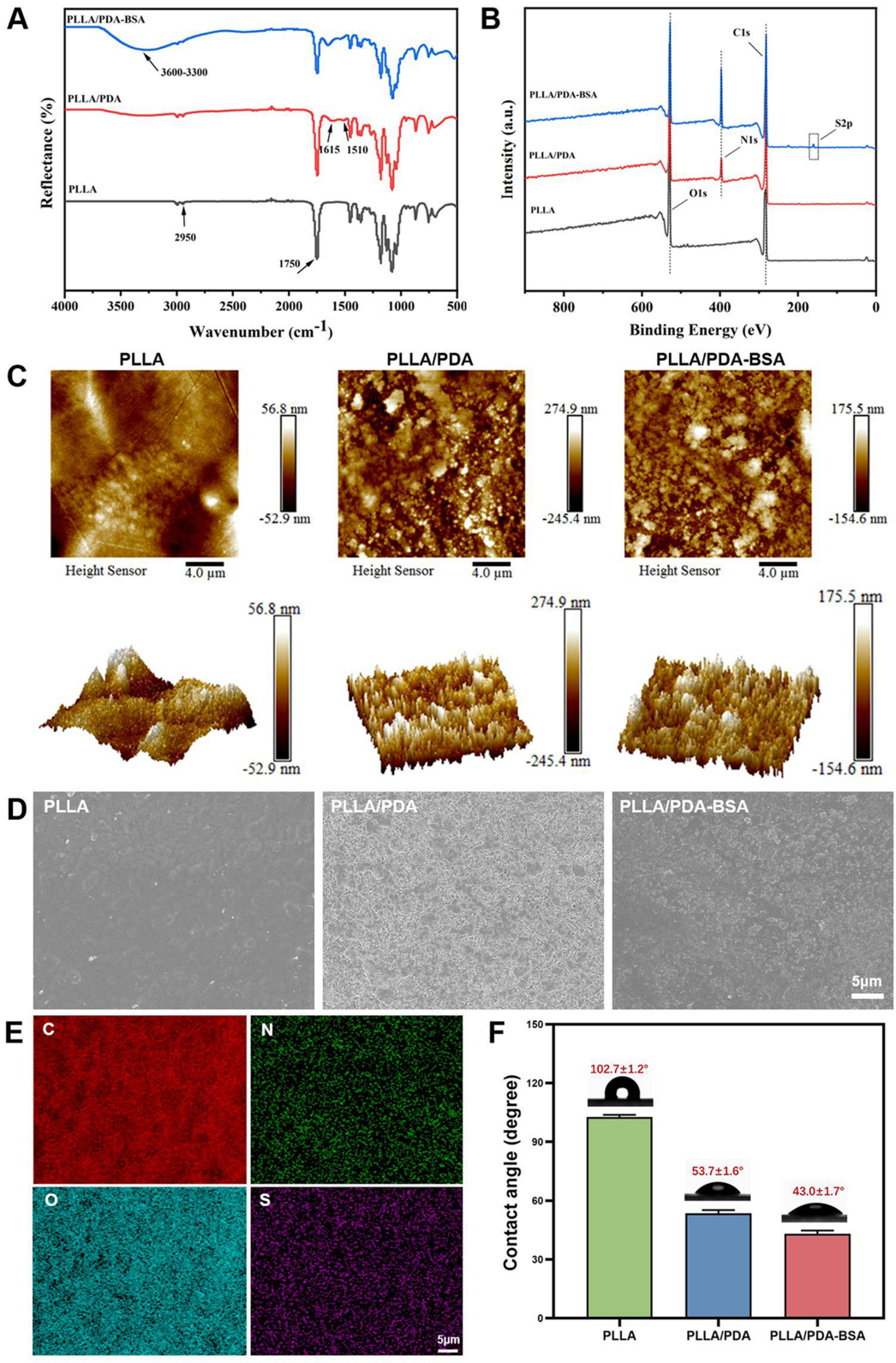

Figure 2 Surface characterization analysis. ATR-FTIR spectra (**A**) and XPS spectra (**B**) and 2D and 3D AFM images (**C**) and SEM images (**D**) of the PLLA, PLLA/PDA and PLLA/PDA-BSA samples. (**E**) EDS mapping images of C, N, O, and S elements on the PLLA/PDA-BSA surface. (**F**) Water contact angle of the samples (mean ± SD, n = 3).

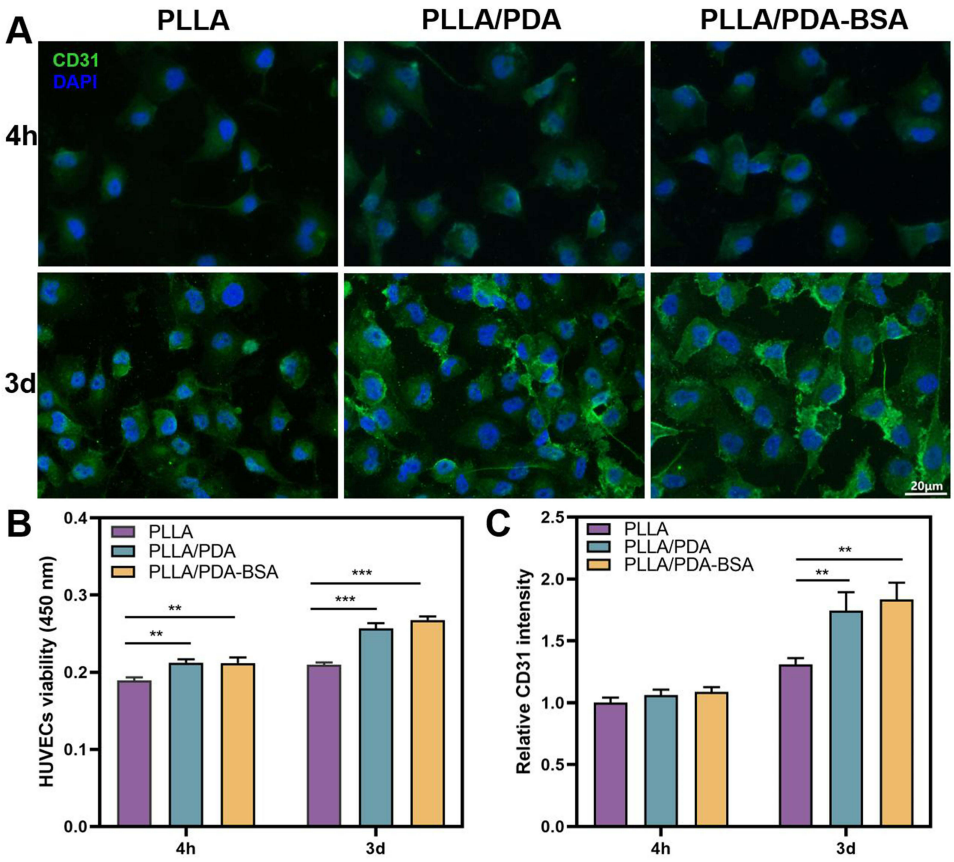

Figure 3 CD31 and DAPI fluorescence staining images (**A**) and relative fluorescence intensities indicating cell viability (**B**) and CD31 expression (**C**) in ECs after 4 h and 3 days on PLLA, PLLA/PDA and PLLA/PDA-BSA samples (n = 3, *p < 0.05, **p < 0.01, ***p < 0.001).

fluorescence intensity, and the CD31 expression levels in ECs on PLLA/PDA and PLLA/PDA-BSA surfaces were significantly greater than those in the PLLA group (Figure 3C), indicating that EC function was improved. Recent research suggests that the poor affinity of PLLA materials for ECs is closely related to their surface hydrophobicity and lack of reactive energy groups.[40] PDA and PDA-BSA coating modifications significantly increased the surface hydrophilicity of PLLA (Figure 2F) and introduced many reactive groups (eg, phenol hydroxyl, primary amino, and quinone groups) on its surface.[41,42] Thus, the PDA-BSA coating improved the affinity of PLLA for ECs, possibly because the hydrophilicity and reactive groups on the surface are more favorable for ECs adhesion and growth.

In vitro and in vivo Inflammatory Responses

Early inflammatory responses that occur after biomaterials are implanted are important factors that lead to immune rejection. The inflammatory response begins with the adhesion and activation of macrophages on the implant surface.[34] As reported in previous studies, morphological changes are a direct and feasible way to assess the degree of macrophage activation.[43,44] Specifically, unactivated macrophages are round or oval in shape, whereas activated macrophages have extended pseudopods and exhibit an amoeba-like irregular shape or an elongated spindle shape.[45] These activated macrophages tend to secrete large amounts of pro-inflammatory factors, which exacerbates this pathological process.[46,47] As shown in Figure 4A, many more macrophages adhered to the PLLA samples than the PLLA/PDA and PLLA/PDA-BSA samples. In addition, the macrophages extended pseudopods and frontal cytoplasmic fringe or showed irregular shapes on the PLLA surfaces, whereas fewer pseudopods extended or rounded shape emerged for macrophages on the PLLA/PDA and PLLA/PDA-BSA surfaces. Enzyme-linked immunosorbent assay (ELISA) analysis (Figure 4B) showed that macrophages secreted significantly less inflammatory factor TNF-α in the PLLA/PDA and PLLA/PDA-BSA

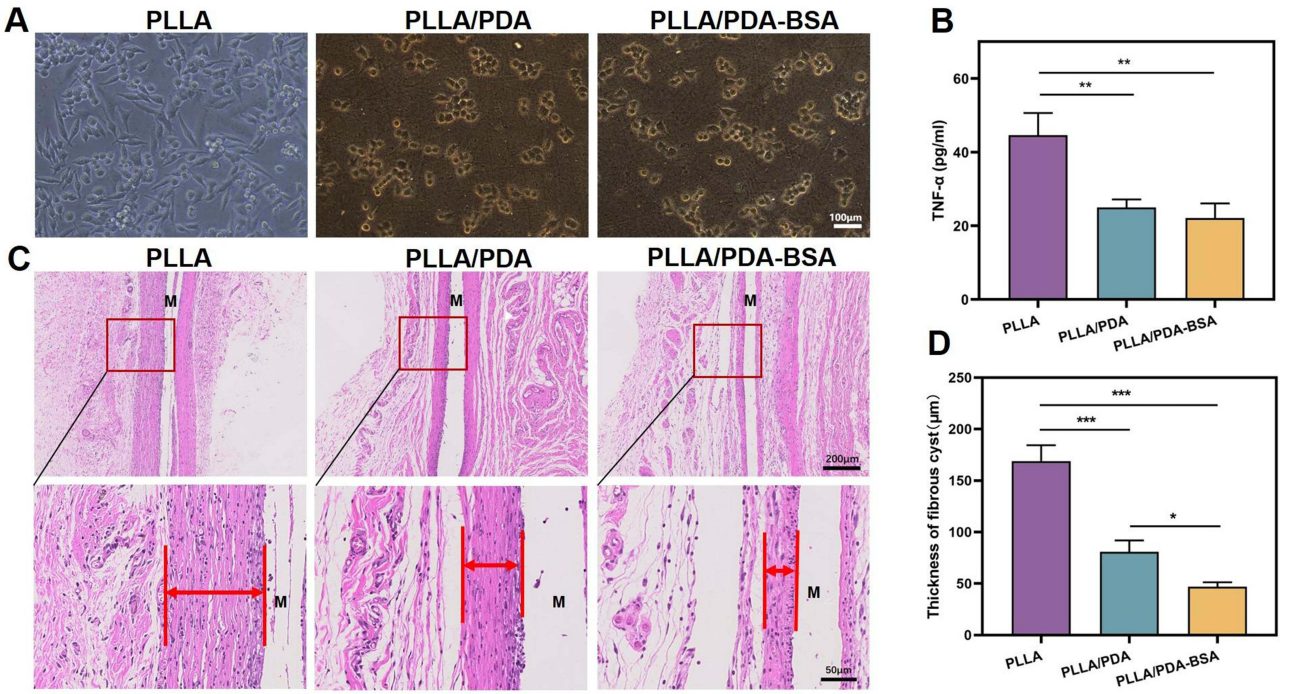

Figure 4 Assessment of the inflammatory response. (**A**) Light microscopy images of macrophages adhering to PLLA, PLLA/PDA, and PLLA/PDA-BSA samples for 3 days; (**B**) ELISA analysis of 3 days TNF-α levels in macrophages from each group. (**C**) H&E staining of the samples 28 days after subcutaneous implantation (M represents the sample implantation location). (**D**) Thickness of the fiber capsule on the surface of subcutaneously implanted samples (n = 3, *p < 0.05, **p < 0.01, ***p < 0.001).

groups than in the PLLA group. These results suggest that the PDA and PDA-BSA coatings have potential antiadhesion effects on macrophages in vitro.

To further evaluate the anti-inflammatory effects of the coating, we performed subcutaneous implantation in SD rats and analyzed the in vivo inflammatory response. It is generally accepted that the greater the degree of inflammatory cell infiltration around the implant, the greater the proliferation of granulation tissue, and the thicker the fibrous capsule, the more severe the inflammatory response of the tissue. The samples were implanted subcutaneously into the backs of Sprague–Dawley (SD) rats for 28 days and then removed to perform H&E staining with the surrounding tissue (Figure 4C). Quantitative analysis (Figure 4D) revealed that the fibrous capsule around PLLA was 169 ± 15 μm thick and was reduced to 81 ± 11 μm after PDA coating modification. However, the fibrous capsule around PLLA/PDA-BSA was only 47 ± 4.4 μm thick and caused the lowest inflammatory response. These results suggest that the PDA-BSA coating significantly attenuates the inflammatory response of the tissues surrounding the PLLA implant. This effect may be attributed to the stealth effect of the albumin coating in resisting nonspecific protein adsorption and preventing recognition by inflammatory cells, 25 which ensures long-term implant performance.

Blood Compatibility Assessment

Hemocompatibility is often regarded as the most critical aspect of vascular stent biocompatibility, as adverse effects are not limited to the local area but also affect distant vital organs.[48,49] Platelet adhesion and activation are important indicators for evaluating the antithrombotic properties of blood contact materials.[50] Platelet morphology has been reported to correlate with platelet activation, and platelets adhered to the surface of a foreign body can usually be classified into the following shapes: round, dendritic, dendritic stretched, stretched, and fully stretched (with increasing activation in that order).[51] SEM (Figure 5A) was used to observe the morphology and number of platelets on the sample surfaces, and the Lactate Dehydrogenase (LDH) Release Assay Kit was used to quantify platelet adherence to the surface of a foreign body by evaluating LDH in the samples; this was performed by assessing LDH activity to quantify the adherent platelets (Figure 5B). The results showed that many platelets adhered to the PLLA surface; However, there was

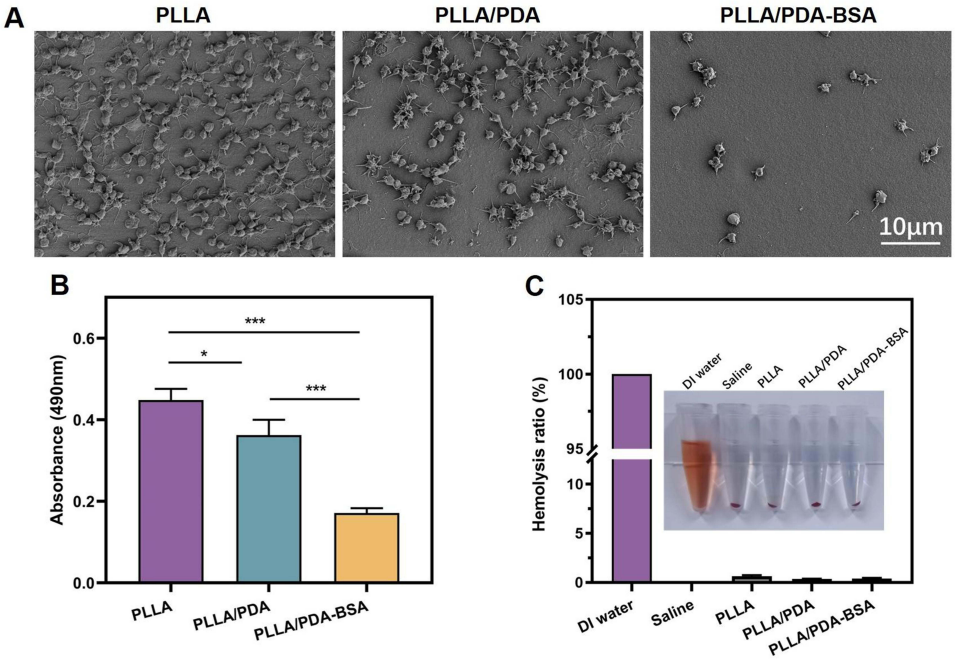

Figure 5 (**A**) SEM images of platelet adhesion on PLLA, PLLA/PDA and PLLA/PDA-BSA surfaces. (**B**) Platelet adhesion on the samples was determined by LDH assay. (**C**) Hemolysis rates of different samples (n = 3, *p < 0.05, ***p < 0.001).

a decrease in platelet adherence on the PLLA/PDA surface, and the platelets that adhered to the PLLA and PLLA/PDA surfaces were significantly activated. The morphology was mainly characterized by dendritic extension and fully extended shapes. However, the number of platelets adhered to the PLLA/PDA-BSA surface was the lowest, and most of the adhered platelets were round with only a few protruding filamentous pseudopods; thus, the platelets were only in the early stage of activation. These results indicate that the PDA-BSA coating achieves excellent performance in preventing platelet adhesion and activation. The hemolysis assay detects the destruction of erythrocytes by the samples, and the results are shown in Figure 5C. In this figure, all samples were below and within the internationally permitted 5% level,[52] indicating the safety of using these coatings as blood contact materials.

To further analyze the antithrombotic effects of the coatings on physiological blood flow, an in vitro blood circulation model was created with rabbits (Figure 6A). After 2 h of circulation, the PLLA and PLLA/PDA membranes induced severe thrombi, whereas a very small amount of thrombus was observed on the PLLA/PDA-BSA membranes (Figure 6B and C). As shown in SEM images (Figure 6D), the surfaces of the PLLA and PLLA/PDA membranes contained many thrombi composed of activated platelets, erythrocytes, and fibrin networks, whereas the surfaces of the PLLA/PDA-BSA membranes contained a small number of erythrocytes with no significant activation of platelets or fibrin networks. In addition, the surface of the PLLA/PDA-BSA membranes contained a small number of erythrocytes with no significant activation of platelets or fibrin networks, and the BSA membranes contained a small number of erythrocytes without significantly activated platelets or fibrin networks. To statistically analyze the anticoagulant effect of the coatings, quantitative analysis was performed by measuring the rate of loop occlusion, the weight of thrombi on the sample surface, and the loop blood flow rate. Quantitative analysis of lumen occlusion (Figure 6E) revealed that the catheter occlusion rates were 86.0±4.6% and 75.3%±6.4% for the curled PLLA and PLLA/PDA membranes, respectively, whereas the occlusion rate for the PLLA/PDA-BSA membrane was only 11.7±2.5%. The weight of thrombus on the surface of the samples is shown in Figure 6F, where the weight of thrombus on the surface of PLLA and PLLA/PDA membranes was 49.2±4.0 mg and 42.2±3.5 mg, respectively, whereas the weight of thrombus on the surface of PLLA/PDA-BSA membranes was only 9.4±2.5 mg. As thrombus formation reduces the lumen flow velocity of the tubes, the PLLA and PLLA/PDA membranes had lumen flow velocities of 15.4±3.3% and 20.1±3.1% of the initial values, respectively, whereas the lumen of the PLLA/PDA-BSA membranes maintained a flow velocity of 88.0±2.9%

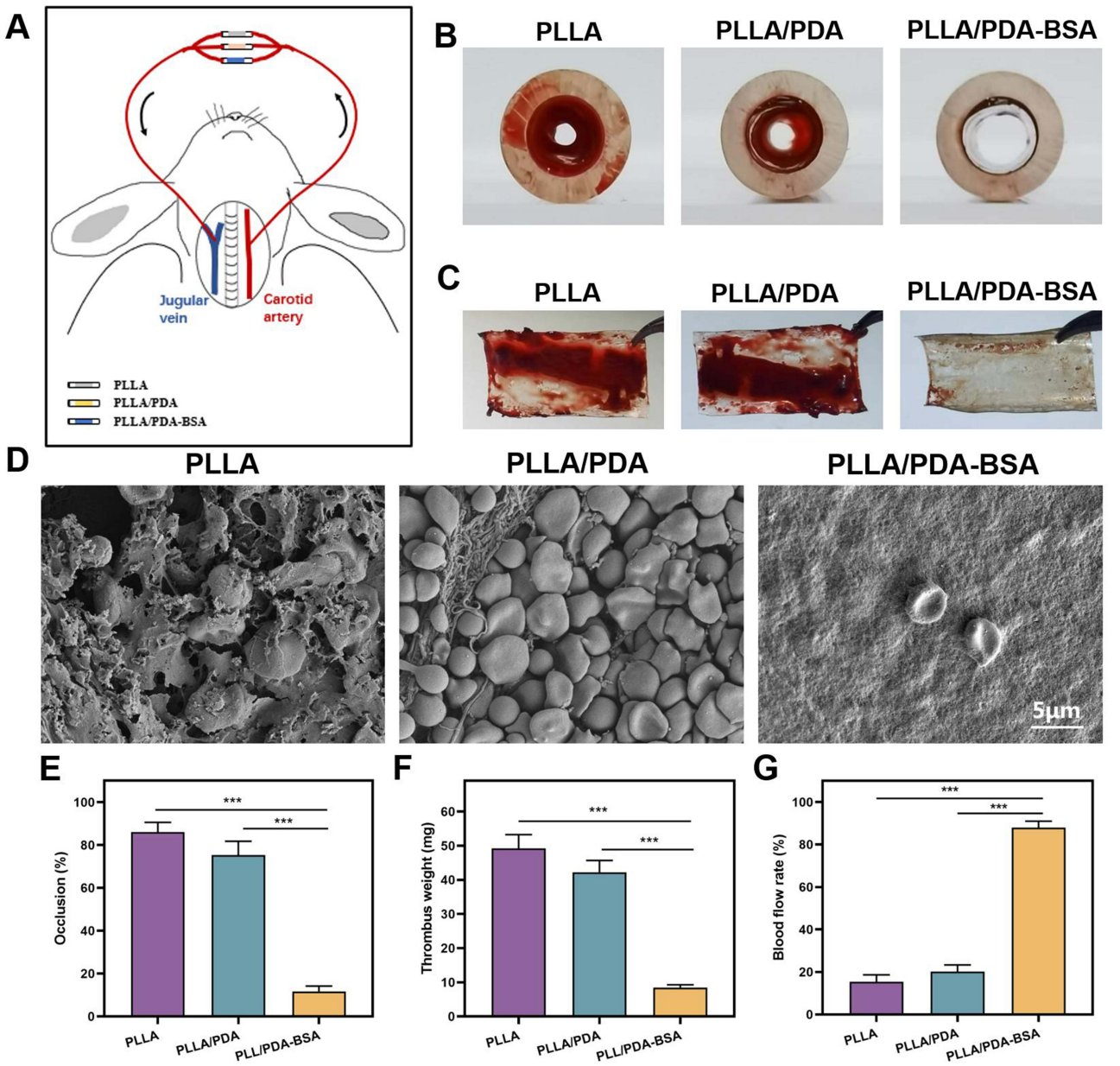

Figure 6 (**A**) Schematic of the in vitro blood circulation model in rabbits. (**B**) Photographs showing the cross-sections of ducts containing PLLA, PLLA/PDA and PLLA/PDA-BSA films. (**C**) Photographs showing thrombus formation on the samples. (**D**) SEM image of a thrombus on the surface of the film. (**E**) Observation rate of the pipe. (**F**) Weights of thrombi on the surface of the sample. (**G**) Blood flow rates in different circuits at the end of extracorporeal circulation (n = 3, ***p < 0.001).

(Figure 6G). These results indicated that the PDA-BSA coating exhibited desirable antithrombotic ability and should meet the high anticoagulant requirements of vascular stents.

A variety of factors affect the hemocompatibility of blood contact materials, such as hydrophilicity/hydrophobicity, surface functional groups, and morphology.[53,54] The hydrophobic surfaces of PLLA materials promote fibrinogen adhesion and conformational changes, which often trigger platelet adhesion. The oxidative self-polymerization of dopamine on the PLLA surface formed a PDA coating, which greatly enhanced the hydrophilicity; however, the increase in surface roughness and the large number of positively charged functional groups induced fibrinogen and platelet adhesion. The immobilization of BSA further enhanced the hydrophilicity of PLLA/PDA and reduced the surface roughness; in addition, albumin has a negative charge at physiological pH,[55] which may inhibit fibrinogen adsorption

and platelet adhesion. Thus, these factors may explain the optimal anticoagulant and blood compatibility effects exhibited by PDA-BSA coating stealth efficacy.

In vivo Vascular Biocompatibility Assessment: Monofilament Sample Implantation

To further investigate the biocompatibility of the PDA-BSA coatings in the vasculature, PLLA, PLLA/PDA, and PLLA/PDA-BSA monofilaments were implanted into the carotid arteries of SD rats. Twenty-eight days after implantation, vascular patency was assessed noninvasively using MRI, and the carotid arteries were subsequently stained with H&E, anti-CD31, anti-α-SMA, and anti-OPN for histological analysis, as shown in Figure 7. The MRI results showed that the vessels implanted with PLLA and PLLA/PDA monofilaments exhibited a more severe degree of occlusion, with obvious

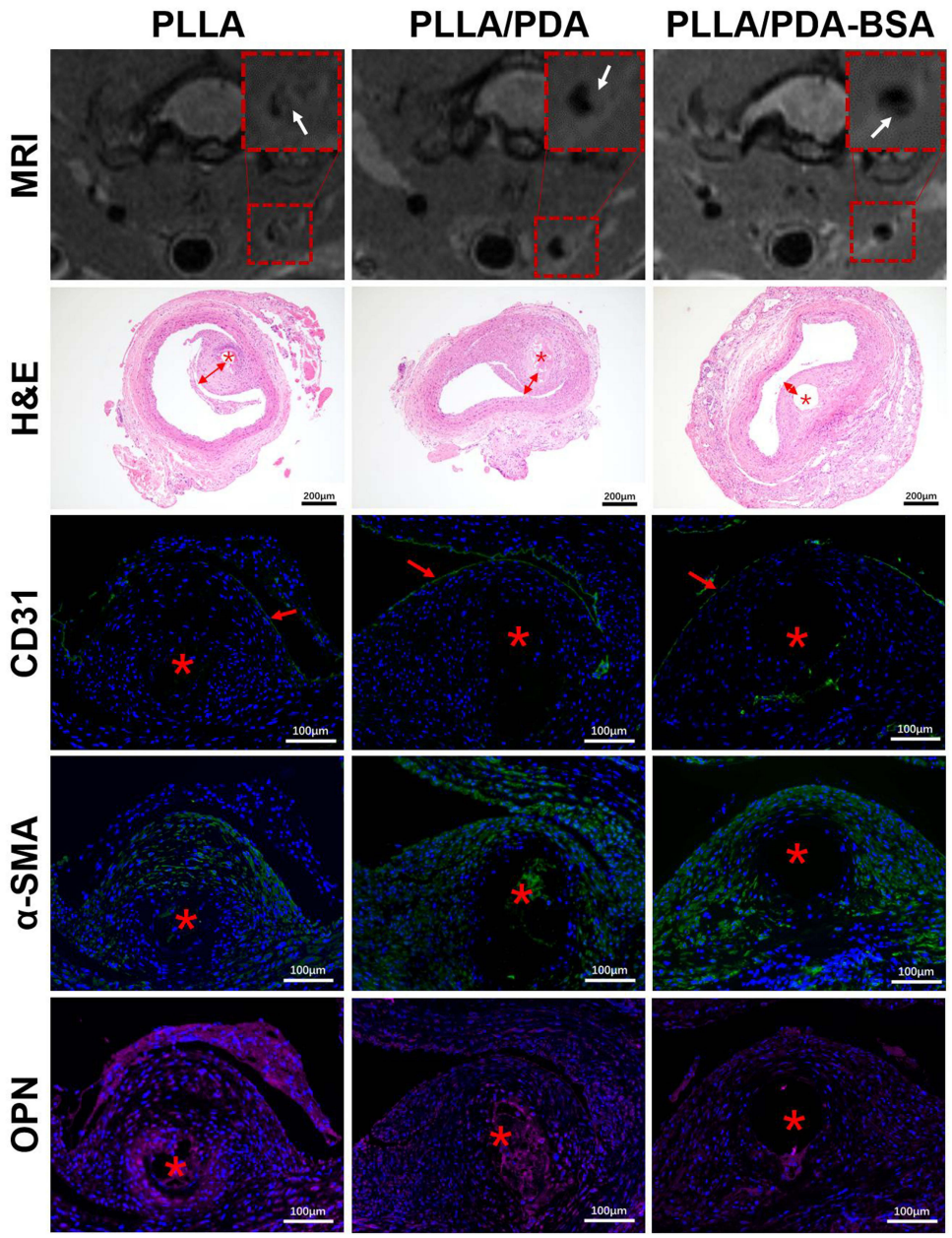

Figure 7 Typical MRI (MSME-PD-T2 sequences) and H&E, anti-CD31 antibody, anti-α-SMA antibody, and anti-OPN antibody staining images of the carotid arteries of Sprague–Dawley (SD) rats implanted with PLLA, PLLA/PDA, or PLLA/PDA-BSA monofilaments for 28 days. (White arrows in red boxes in MRI vessel wall images indicate proliferative tissue; red bidirectional arrows in H&E-stained images represent the thickness of the neointimal hyperplasia; red unidirectional arrows in anti-CD31 antibody-stained images indicate the endothelial layer of the neointimal hyperplasia; and red *Marks the location of each implanted sample.).

hyperplastic tissue visible in the lumen; in contrast, the vessels implanted with PLLA/PDA-BSA monofilaments had the least severe degree of occlusion, with only fine thread-like hyperplastic tissue visible in the lumen. H&E staining revealed that the PLLA (175.5±8.6 μm) and PLLA/PDA (104.6±23.4 μm) groups contained thicker neointima, while the PLLA/PDA-BSA (79.8±11.3μm) group contained thinner neointima. These findings are similar to the MRI results and suggest that the PDA/BSA coating can effectively inhibit neointimal hyperplasia and shows the potential to prevent restenosis. The EC layers of the vascular wall are important for maintaining the homeostasis of the vascular microenvironment; in addition, the layers can synthesize and secrete various bioactive substances to ensure that the blood vessels contract and relax in a normal manner, thus maintaining normal flow and long-term patency.[56] Therefore, we evaluated the effect of the PDA-BSA coating on EC repair. CD31 staining revealed that PDA- and PDA-BSA-coated neointimal surfaces exhibited a better degree of EC coverage than that of PLLA, indicating good surface reendothelialization. The pathological transition of vascular smooth muscle cells (SMCs) from a contractile to a synthetic phenotype causes neointimal hyperplasia and restenosis after stent implantation and is detrimental to reendothelialization and maintenance of endothelial function.[57] α-SMA is a specific marker of contracted SMCs, and OPN is a specific marker of synthesized SMCs.[58] The α-SMA and OPN immunofluorescence staining images indicated that the neointimal hyperplasia around PLLA/PDA and PLLA/PDA-BSA monofilaments exhibited stronger α-SMA (green) and slighter OPN (red) than that around PLLA, suggesting that SMCs are better regulated from a synthetic phenotype to a contractile phenotype or maintain their contractile phenotype. Taken together, the results suggest that PDA/BSA coating promotes the reendothelialization of the neointimal around PLLA monofilaments, maintains the contractile phenotype of SMCs and reduces neointimal hyperplasia, which effectively demonstrates the potential of this coating for the application of PLLA vascular stents.

In summary, our research has shown that the application of PDA-BSA coating significantly improves the biocompatibility of PLLA stent materials. However, it is also essential to consider the stability and degradability of PLLA stents as critical factors for their successful clinical application. Literatures reported that absorbable stents are expected to provide adequate radial support to diseased vessels for a minimum of 6 months post-implantation to facilitate the remodeling of stenotic vessels.[59] It typically takes between two and three years for PLLA stents to be fully absorbed by the body.[60] Early degradation, which negatively affects their mechanical properties, is not conducive to maintaining the early supportive role of the stent.[61,62] In our 28-day small animal model, intact PLLA monofilaments were still discernible during the pathological sampling process, indicating that significant degradation or stability alterations may not have occurred during the short implantation period. The PDA-BSA coating serves as a physical barrier on the surface of the PLLA, potentially slowing down the degradation of PLLA stents and maintaining early mechanical properties. Therefore, further research involving long-term large animal experiments is needed to comprehensively assess the in vivo biological performance of PDA-BSA coating-modified PLLA stents.

Conclusion

This study describes the successful construction of a biomimetic albumin (PDA-BSA) coating on the surface of PLLA materials using a mussel-inspired surface modification technique. This technique provides an effective pathway for the functionalization of surface albumin with PLLA, which lacks reactive groups. The PDA-BSA coating exhibited excellent anti-thrombogenic and anti-inflammatory properties, significantly attenuating the foreign body reactions caused by the PLLA materials. These results highlight the role of surface albumin coating in producing a stealth effect. Intravascular implantation experiments demonstrated favorable biocompatibility on this surface, which protected against neointimal hyperplasia, promoted endothelial repair and maintained the SMC contractile phenotype. These results demonstrated the great potential of the PDA-BSA coating as a multifunctional biointerface, which is expected to significantly improve the biocompatibility of PLLA stents. In the future, the properties and application potential of these coatings should be studied in a more in-depth and comprehensive manner to provide deeper insights and guidance for the development of medical devices related to vascular implants.

Acknowledgments

The authors would like to thank the Jiangsu Province Science and Technology Support Project (No.: BE2023769) and National Key Research and Development Programs (Nos.: 2018YFA0704100 and 2018YFA0704104) for financially supporting this research. The authors thank Figdraw (www.figdraw.com) for providing materials for the graphical abstract.

Disclosure

The authors reports no conflicts of interest in this work.

References

1. Tsao CW, Aday AW, Almarzooq ZI, et al. Heart disease and stroke statistics-2022 update: a report from the American Heart Association. *Circulation*. 2022;145(8):E153–E639. doi:10.1161/CIR.0000000000001052
2. Bangalore S, Guo Y, Samadashvili Z, Blecker S, Xu JF, Hannan EL. Everolimus-eluting stents or bypass surgery for multivessel coronary disease. *N Engl J Med*. 2015;372(13):1213–1222. doi:10.1056/NEJMoa1412168
3. Ahn JM, Kang DY, Yun SC, et al. Everolimus-eluting stents or bypass surgery for multivessel coronary artery disease: extended follow-up outcomes of multicenter randomized controlled BEST trial. *Circulation*. 2022;146(21):1581–1590. doi:10.1161/CIRCULATIONAHA.122.062188
4. Joner M, Finn AV, Farb A, et al. Pathology of drug-eluting stents in humans - Delayed healing and late thrombotic risk. *J Am Coll Cardiol*. 2006;48 (1):193–202. doi:10.1016/j.jacc.2006.03.042
5. Torii S, Jinnouchi H, Sakamoto A, et al. Drug-eluting coronary stents: insights from preclinical and pathology studies. *Nat Rev Cardiol*. 2020;17 (1):37–51. doi:10.1038/s41569-019-0234-x
6. Bonaa KH, Mannsverk J, Wiseth R, et al. Drug-eluting or bare-metal stents for coronary artery disease. *N Engl J Med*. 2016;375(13):1242–1252. doi:10.1056/NEJMoa1607991
7. Hickethier T, Kröger JR, Von Spiczak J, et al. Non-invasive imaging of bioresorbable coronary scaffolds using CT and MRI: first in vitro experience. *Int J Cardiol*. 2016;206:101–106. doi:10.1016/j.ijcard.2016.01.028
8. Peng X, Qu WB, Jia Y, Wang YN, Yu B, Tian JW. Bioresorbable scaffolds: contemporary status and future directions. *Front Cardiovasc Med*. 2020;7. doi:10.3389/fcvm.2020.589571
9. Lasprilla AJR, Martinez GAR, Lunelli BH, Jardini AL, Maciel R. Poly-lactic acid synthesis for application in biomedical devices - A review. *Biotechnol Adv*. 2012;30(1):321–328. doi:10.1016/j.biotechadv.2011.06.019
10. Ormiston JA, Serruys PW, Regar E, et al. A bioabsorbable everolimus-eluting coronary stent system for patients with single de-novo coronary artery lesions (ABSORB): a prospective open-label trial. *Lancet*. 2008;371(9616):899–907. doi:10.1016/S0140-6736(08)60415-8
11. Serruys PW, Ormiston JA, Onuma Y, et al. A bioabsorbable everolimus-eluting coronary stent system (ABSORB): 2-year outcomes and results from multiple imaging methods. *Lancet*. 2009;373(9667):897–910. doi:10.1016/S0140-6736(09)60325-1
12. Song Y, Li B, Chen H, Yu Z. Research progress of absorbable stents. *Int J Med Sci*. 2024;21(2):404–412. doi:10.7150/ijms.90012
13. Zoppo CT, Mocco J, Manning NW, Bogdanov AA, Gounis MJ. Surface modification of neurovascular stents: from bench to patient. *J Neurointervent Surg*. 2023;jnis-2023–020620. doi:10.1136/jnis-2023-020620
14. Kim HI, Ishihara K, Lee S, et al. Tissue response to poly(L-lactic acid)-based blend with phospholipid polymer for biodegradable cardiovascular stents. *Biomaterials*. 2011;32(9):2241–2247. doi:10.1016/j.biomaterials.2010.11.067
15. Arques S. Human serum albumin in cardiovascular diseases. *Eur J Internal Med*. 2018;52:8–12. doi:10.1016/j.ejim.2018.04.014
16. Pella OK, Hornyák I, Horváthy D, Fodor E, Nehrer S, Lacza Z. Albumin as a biomaterial and therapeutic agent in regenerative medicine. *Int J Mol Sci*. 2022;23(18):10557.
17. Cui JW, He S, Dai S, et al. Stepwise assembly of functional proteins on Photo-activated TiO2 surfaces confers anti-oxidative stress ability and stealth effect to vascular stents. *Chem Eng J*. 2021;424:130392. doi:10.1016/j.cej.2021.130392
18. Bilek MM, Bax DV, Kondyurin A, et al. Free radical functionalization of surfaces to prevent adverse responses to biomedical devices. *Proc Natl Acad Sci U S A*. 2011;108(35):14405–14410. doi:10.1073/pnas.1103277108
19. Park JH, Jackman JA, Ferhan AR, Ma GJ, Yoon BK, Cho NJ. Temperature-induced denaturation of BSA protein molecules for improved surface passivation coatings. *ACS Appl Mater Interfaces*. 2018;10(38):32047–32057. doi:10.1021/acsami.8b13749
20. Xu XH, Hu JY, Xue HQ, et al. Applications of human and bovine serum albumins in biomedical engineering: a review. *Int J Biol Macromol*. 2023;253:126914. doi:10.1016/j.ijbiomac.2023.126914
21. Sato H, Nakhaei E, Kawano T, et al. Ligand-mediated coating of liposomes with human serum albumin. *Langmuir*. 2018;34(6):2324–2331. doi:10.1021/acs.langmuir.7b04024
22. Auvinen H, Zhang HB, Nonappa, et al. Protein coating of DNA nanostructures for enhanced stability and immunocompatibility. *Adv. Healthcare Mater*. 2017;6(18). doi:10.1002/adhm.201700692
23. Yu J, Ju YM, Zhao LY, et al. Multistimuli-regulated photochemothermal cancer therapy remotely controlled via Fe5C2 nanoparticles. *ACS Nano*. 2016;10(1):159–169. doi:10.1021/acsnano.5b04706
24. Kenry, Loh KP, Lim CT. Molecular hemocompatibility of graphene oxide and its implication for antithrombotic applications. *Small*. 2015;11 (38):5105–5117. doi:10.1002/smll.201500841
25. Tao C, Zhu WZ, Iqbal J, Xu CJ, Wang DA. Stabilized albumin coatings on engineered xenografts for attenuation of acute immune and inflammatory responses. *J Mat Chem B*. 2020;8(28):6080–6091. doi:10.1039/D0TB01111H
26. Sprott MR, Gallego-Ferrer G, Dalby MJ, Salmerón-Sánchez M, Cantini M. Functionalization of PLLA with polymer brushes to trigger the assembly of fibronectin into nanonetworks. *Adv. Healthcare Mater*. 2019;8(3). doi:10.1002/adhm.201801469
27. Lee H, Dellatore SM, Miller WM, Messersmith PB. Mussel-inspired surface chemistry for multifunctional coatings. *Science*. 2007;318 (5849):426–430. doi:10.1126/science.1147241
28. Cheng W, Zeng X, Chen H, et al. Versatile polydopamine platforms: synthesis and promising applications for surface modification and advanced nanomedicine. *ACS Nano*. 2019;13(8):8537–8565. doi:10.1021/acsnano.9b04436
29. Zhang X, Chen J, Brott BC, et al. Pro-healing nanomatrix-coated stent analysis in an in vitro vascular double-layer system and in a rabbit model. *ACS Appl Mater Interfaces*. 2022;14(46):51728–51743. doi:10.1021/acsami.2c15554
30. Yang Z, Tu Q, Zhu Y, et al. Mussel-inspired coating of polydopamine directs endothelial and smooth muscle cell fate for re-endothelialization of vascular devices. *Adv. Healthcare Mater*. 2012;1(5):548–559. doi:10.1002/adhm.201200073
31. Diaz-Rodriguez S, Rasser C, Mesnier J, et al. Coronary stent CD31-mimetic coating favours endothelialization and reduces local inflammation and neointimal development in vivo. *Eur Heart J*. 2021;42(18):1760–1769. doi:10.1093/eurheartj/ehab027

32. Ryu JH, Messersmith PB, Lee H. Polydopamine surface chemistry: a decade of discovery. *ACS Appl Mater Interfaces*. 2018;10(9):7523–7540. doi:10.1021/acsami.7b19865
33. Zhao GT, Li X, Tian Y, et al. Poly(L-lactic acid) monofilaments for biodegradable braided self-expanding stent. *J Mater Sci*. 2021;56 (21):12383–12393. doi:10.1007/s10853-021-06021-x
34. Lu J, Zhuang WH, Li LH, et al. Micelle-embedded layer-by-layer coating with catechol and phenylboronic acid for tunable drug loading, sustained release, mild tissue response, and selective cell fate for re-endothelialization. *ACS Appl Mater Interfaces*. 2019;11(10):10337–10350. doi:10.1021/acsami.9b01253
35. Xue W, Nasr SH, Guan GP, et al. An efficient surface modification strategy improving endothelialization with polydopamine nanoparticles and REDV peptides for stent-grafts. *ACS Appl Bio Mater*. 2019;2(9):3820–3827. doi:10.1021/acsabm.9b00421
36. Yang F, Guo GY, Wang YB. Inflammation-directed nanozyme-eluting hydrogel coating promotes vascular tissue repair by restoring reactive oxygen species homeostasis. *Chem Eng J*. 2023;454:140556. doi:10.1016/j.cej.2022.140556
37. Hou YC, Li JA, Zhu SJ, et al. Tailoring of cardiovascular stent material surface by immobilizing exosomes for better pro-endothelialization function. *Colloids Surf B Biointerfaces*. 2020;189:110831. doi:10.1016/j.colsurfb.2020.110831
38. Curcio A, Torella D, Indolfi C. Mechanisms of smooth muscle cell proliferation and endothelial regeneration after vascular injury and stenting - approach to therapy. *Circ J*. 2011;75(6):1287–1296. doi:10.1253/circj.CJ-11-0366
39. Alfonso F, Sandoval J, Pérez-Vizcayno MJ, et al. Mechanisms of balloon angioplasty and repeat stenting in patients with drug-eluting in-stent restenosis. *Int J Cardiol*. 2015;178:213–220. doi:10.1016/j.ijcard.2014.10.139
40. Xu H, Deshmukh R, Timmons R, Kytai TN. Enhanced endothelialization on surface modified Poly(L-Lactic Acid) substrates. *Tissue Eng Part A*. 2011;17(5–6):865–876. doi:10.1089/ten.tea.2010.0129
41. Li H, Chen C, Li ZM, et al. Specific interaction with human serum albumin reduces ginsenoside cytotoxicity in human umbilical vein endothelial cells. *Front Pharmacol*. 2020;11:498. doi:10.3389/fphar.2020.00498
42. Jiang Y, Wang H, Wang X, Li Q. Surface modification with hydrophilic and heparin-loaded coating for endothelialization and anticoagulation promotion of vascular scaffold. *Int J Biol Macromol*. 2022;219:1146–1154. doi:10.1016/j.ijbiomac.2022.08.172
43. Saino E, Focarete ML, Gualandi C, et al. Effect of electrospun fiber diameter and alignment on macrophage activation and secretion of proinflammatory cytokines and chemokines. *Biomacromolecules*. 2011;12(5):1900–1911. doi:10.1021/bm200248h
44. Yi BC, Yu L, Tang H, Wang WB, Liu W, Zhang YZ. Lysine-doped polydopamine coating enhances antithrombogenicity and endothelialization of an electrospun aligned fibrous vascular graft. *Appl Mater Today*. 2021;25:101198. doi:10.1016/j.apmt.2021.101198
45. Yang L, Wu HS, Liu YQ, et al. A robust mussel-inspired zwitterionic coating on biodegradable poly (L-lactide) stent with enhanced anticoagulant, anti-inflammatory, and anti-hyperplasia properties. *Chem Eng J*. 2022;427:130910. doi:10.1016/j.cej.2021.130910
46. Lee HS, Stachelek SJ, Tomczyk N, Finley MJ, Composto RJ, Eckmann DM. Correlating macrophage morphology and cytokine production resulting from biomaterial contact. *J Biomed Mater Res Part A*. 2013;101(1):203–212. doi:10.1002/jbm.a.34309
47. Refai AK, Textor M, Brunette DM, Waterfield JD. Effect of titanium surface topography on macrophage activation and secretion of proinflammatory cytokines and chemokines. *J Biomed Mater Res Part A*. 2004;70A(2):194–205. doi:10.1002/jbm.a.30075
48. Wang Y, Lan HL, Yin TY, et al. Covalent immobilization of biomolecules on stent materials through mussel adhesive protein coating to form biofunctional films. *Mater Sci Eng C Mater Biol Appl*. 2020;106:110187. doi:10.1016/j.msec.2019.110187
49. Liu HQ, Pan CJ, Zhou SJ, Li JF, Huang N, Dong LH. Improving hemocompatibility and accelerating endothelialization of vascular stents by a copper-titanium film. *Mater Sci Eng C Mater Biol Appl*. 2016;69:1175–1182. doi:10.1016/j.msec.2016.08.028
50. Shen YH, Tang CJ, Sun BB, et al. 3D printed personalized, heparinized and biodegradable coronary artery stents for rabbit abdominal aorta implantation. *Chem Eng J*. 2022;450:138202. doi:10.1016/j.cej.2022.138202
51. Luo RF, Zhang J, Zhuang WH, et al. Multifunctional coatings that mimic the endothelium: surface bound active heparin nanoparticles with in situ generation of nitric oxide from nitrosothiols. *J Mat Chem B*. 2018;6(35):5582–5595. doi:10.1039/C8TB00596F
52. Sinn S, Scheuermann T, Deichelbohrer S, Ziemer G, Wendel HP. A novel in vitro model for preclinical testing of the hemocompatibility of intravascular stents according to ISO 10993-4. *J Mater Sci*. 2011;22(6):1521–1528. doi:10.1007/s10856-011-4335-2
53. Dong XH, Yuan XY, Wang LN, et al. Construction of a bilayered vascular graft with smooth internal surface for improved hemocompatibility and endothelial cell monolayer formation. *Biomaterials*. 2018;181:1–14. doi:10.1016/j.biomaterials.2018.07.027
54. Tan X, Gao P, Li YL, et al. Poly-dopamine, poly-levodopa, and poly-norepinephrine coatings: comparison of physico-chemical and biological properties with focus on the application for blood-contacting devices. *Bioact Mater*. 2021;6(1):285–296. doi:10.1016/j.bioactmat.2020.06.024
55. Lei C, Liu XR, Chen QB, et al. Hyaluronic acid and albumin based nanoparticles for drug delivery. *J Control Release*. 2021;331:416–433. doi:10.1016/j.jconrel.2021.01.033
56. Krüger-Genge A, Blocki A, Franke RP, Jung F. Vascular endothelial cell biology: an update. *Int J Mol Sci*. 2019;20(18):4411. doi:10.3390/ijms20184411
57. Li JG, Wu F, Zhang K, et al. Controlling molecular weight of hyaluronic acid conjugated on amine-rich surface: toward better multifunctional biomaterials for cardiovascular implants. *ACS Appl Mater Interfaces*. 2017;9(36):30343–30358. doi:10.1021/acsami.7b07444
58. Choi JS, Piao Y, Seo TS. Circumferential alignment of vascular smooth muscle cells in a circular microfluidic channel. *Biomaterials*. 2014;35 (1):63–70. doi:10.1016/j.biomaterials.2013.09.106
59. Cheng J, Su J, Tian Y, Hu X, Zhao G, Ni Z. Experimental investigation on the properties of poly (L-lactic acid) vascular stent after accelerated in vitro degradation. *J Appl Polym Sci*. 2023;140(1):e53116. doi:10.1002/app.53116
60. Tesfamariam B. Bioresorbable vascular scaffolds: biodegradation, drug delivery and vascular remodeling. *Pharmacol Res*. 2016;107:163–171. doi:10.1016/j.phrs.2016.03.020
61. Zhao GT, Wang B, Li X, et al. Evaluation of poly (L-lactic acid) monofilaments with high mechanical performance in vitro degradation. *J Mater Sci*. 2022;57(11):6361–6371. doi:10.1007/s10853-022-07049-3
62. Park DS, Jeong MH, Jin YJ, et al. Preclinical evaluation of an everolimus-eluting bioresorbable vascular scaffold via a long-term rabbit iliac artery model. *Tissue Eng and Regener Med*. 2023;20(2):239–249. doi:10.1007/s13770-023-00518-z